

A Hadronization Approach of Quark-Gluon Plasma at RHIC

Hong Miao¹, Chongshou Gao², Pengfei Zhuang¹

¹Physics Department, Tsinghua University, Beijing 100084, China and

²School of Physics, Peking University, Beijing 100871, China

A transport model is developed to describe hadron emission from a strongly coupled quark-gluon plasma formed in relativistic heavy ion collisions. The quark-gluon plasma is controlled by ideal hydrodynamics, and the hadron motion is characterized by a transport equation with loss and gain terms. The two sets of equations are coupled to each other, and the hadronization hypersurface is determined by both the hydrodynamic evolution and the hadron emission. The model is applied to calculate the transverse momentum distributions of mesons and baryons, and most of the results agree well with the experimental data at RHIC.

PACS numbers: 12.38.Mh, 25.75.-q

I. INTRODUCTION

The hot and dense matter created in relativistic heavy ion collisions provides the condition to investigate the new state of matter of QCD, the so-called quark-gluon plasma (QGP) [1, 2, 3, 4, 5]. The space-time evolution of QGP and its hadronization process are still open questions in the research of this area. Hydrodynamics [6, 7, 8] based on the assumption of local thermal and chemical equilibrium and models of quark coalescence [9, 10] or recombination [11, 12] and fragmentation [13, 14] are often used to describe the evolution and hadronization of QGP formed in heavy ion collisions at RHIC. However, we do not know a priori if the colliding system can reach equilibrium or not. In fact, because of the very small size and very short lifetime of the collision zone [15, 16, 17], the highly excited system may spend a considerable fraction of the lifetime in a non-equilibrium state [18]. On the other hand, even if the system reaches equilibrium in the early quark-gluon stage, the hadrons formed in the later stage will be in non-equilibrium state, since the particle density in hadron phase is much smaller than that in the parton stage.

Evaporation models [19, 20, 21] developed many years ago are widely used to describe the hadronization of QGP. In some of the models, the emission rate is calculated from a simple assumption of balance between the particle emission and absorption in QGP and in hadron gas at a critical temperature T_c . Under this assumption, the particle emission distribution is just the corresponding ideal thermal distribution of hadron gas, $f(p) = f^T(p)$.

However, considering the feedback effect of hadron evaporation on QGP, the space-time evolution of QGP and hadron evaporation are coupled to each other and the system is governed by both the hydrodynamic expansion and the evaporation. On the other hand, when the expansion of the system is fast, the fluid will be more likely to split into relatively small bubbles during the hadron evaporation. In this case, the system is a mixture of QGP bubbles and physical vacuum, and the energy density of the system is lower than that of a unitary QGP. These

bubbles may provide a mechanism to reduce the viscosity of the system and make it more accessible for the ideal hydrodynamics to work at RHIC [22]. Thirdly, from the analysis of collective flow measured at RHIC [23], the QGP formed at RHIC is a strongly coupled quark-gluon plasma (sQGP) [24, 25, 26, 27] where there exist not only quarks and gluons but also some of their resonant states like qq and qg .

In this paper, we consider an effective hadronization model for the production of soft particles in relativistic heavy ion collisions. In the model, the QGP evolution is described by ideal hydrodynamics together with the equation of state including quarks, gluons and their resonant states. At the critical temperature, the expansion does not change the temperature of the system, and the decrease of the energy density is due to the splitting of the QGP fluid. When the energy density reaches the value for hadronization, which is a free parameter in our calculation, the evaporation starts and the hadron distributions are controlled by transport equations. The evaporation hypersurface is characterized by both the hydrodynamics and the evaporation.

The paper is organized as follows. In Section II we discuss hadron production and transport and derive an approximate emission distribution. In Section III we consider the hydrodynamics for the evolution of QGP with possible splitting into droplets and the effective evaporation boundary condition. We apply our model to hadron spectra in heavy ion collisions at RHIC energy in Section IV. We summarize in Section V.

II. HADRON EMISSION

We investigate in this section the transport of hadrons emitted from QGP. The classical transport equation for the evolution of hadron phase space distribution $f(t; r; p)$ can be written as

$$\frac{\partial f}{\partial t} + v \cdot r f = Q + f; \quad (1)$$

where the second term on the left hand side is the free streaming part, and on the right hand side the loss and

gain terms $(p)f$ and (p) indicate hadron absorption and production in QGP, and the elastic term $Q(p;f)$ [28] controls the thermalization of the hadrons.

Under the assumption of quasi-static condition, the time evolution [29] during the transport can be temporarily removed. If we only focus on a one dimensional hadron transport in the region $x > 0$ and treat the elastic scattering in relaxation time approximation, the hadron transport can be greatly simplified,

$$v \cos \theta \frac{\partial f}{\partial x} = \frac{f - f^T}{\tau} + \dots \quad (2)$$

where $v = p/E$ is the hadron velocity, τ the relaxation time parameter, and $f^T(p)$ the thermal hadron distribution. In principle, τ should depend on the hadron momentum and the type of hadrons. For simplicity, we take it as a universal constant in our global model. Considering the finite volumes of hadrons and resonances, the phase space distribution will be suppressed. An effective way to include the volume effect in the thermal distribution is to multiply f^T by a factor $1 - y_0$, where y_0 is the ratio of the occupation volume of all the excluded hadrons to the whole volume of the system [30, 31]. In the following calculation we will always consider this volume effect for f^T .

The transport equation (2) can be solved with the analytic result

$$f(x; p) = f_1(p) + [f(0; p) - f_1(p)] e^{-\frac{(p) + 1}{v \cos \theta} x} \quad (3)$$

with $f_1(p)$ defined as

$$f_1(p) = \frac{f^T(p) + (p)}{(p) + 1} \quad (4)$$

It is easy to see that the hadrons reach chemical equilibrium in the limit of vanishing inelastic interactions with $(p) = 0$ and thermal equilibrium in the limit of infinitely strong elastic interaction with $(p) = 0$. In the both cases, the distribution at $x \rightarrow \infty$ is reduced to the thermal one,

$$f_1(p) = f^T(p) \quad (5)$$

Taking into account the boundary condition at $x = 0$,

$$f(0; p) = 0; \quad (\cos \theta > 0); \quad (6)$$

which means no hadrons moving from the vacuum in the region of $x < 0$ to the QGP phase in the region of $x > 0$, and the constraint

$$0 \leq f(x; p) \leq f_1(p); \quad (7)$$

the hadron distribution can be expressed as

$$f(x; p) = f_1(p) \theta(x) e^{-\frac{(p) + 1}{v \cos \theta} x}; \quad (8)$$

where $\theta(x)$ is a step function.

It can be seen from the above discussion that the influence of the transport process is mainly reflected in the region near the QGP surface at $x = 0$. Most of the emitted hadrons are created in this region. Since the energy density in the inner part of the QGP fluid is higher than the value on the surface, the hadronization of the QGP fluid can be effectively regarded as a surface evaporation.

In the above derivation we did not consider the QGP surface shift and the breaking of the fluid in the process of hadron emission. A simple way to take the surface shift and fluid splitting into account is to introduce two parameters v_s and γ in the model. The former is the shrinking velocity of the surface, and the latter is the ratio of the occupation volume of all the QGP droplets to the whole volume of the system. These two parameters should be considered simultaneously in the transport equation for hadron emission and the hydrodynamic equation for QGP evolution. With these two parameters, the hadron transport equation can be effectively written as

$$(v \cos \theta - v_s) \frac{\partial f}{\partial x} = \frac{f - f^T}{\tau} + \dots \quad (9)$$

with the solution

$$f(x; p) = \frac{f_1(p)}{1 - \gamma} e^{-\frac{(p) + 1}{(v \cos \theta - v_s) \tau} x} \quad (10)$$

With the hadron distribution, the energy loss of the QGP fluid in the rest frame of the boundary can be expressed as

$$\frac{dE}{dt dS} = \sum_i \int_{\Omega} f_1^i(p_i) (v_i \cos \theta - v_s) E_i d^3 p_i; \quad (11)$$

where the integration over the angle θ is restricted by the condition $v_i \cos \theta - v_s < 0$, E_i is the energy of a hadron of type i , and the summation runs over all the hadron types. Similarly, the momentum loss of the QGP fluid can be written as

$$\frac{dP}{dt dS} = \sum_i \int_{\Omega} f_1^i(p_i) (v_i \cos \theta - v_s) p \cos \theta d^3 p_i; \quad (12)$$

If hydrodynamic expansion is neglected, the equation

$$\frac{dE}{dt dS} = \gamma \epsilon \quad (13)$$

defines a minimal shrinking velocity of the fluid, where ϵ is the average energy density at the boundary. When γ is small enough to make $v_s = 1$, the local association between different parts of the fluid will completely vanish, and the fluid must decouple. Therefore, the condition for the fluid description of the system is that the energy density must satisfy

$$\frac{dE}{dt dS} \geq \gamma \epsilon_{v_s=1} \quad (14)$$

The question left for the emission distribution of hadrons is the determination of the loss and gain terms and . We first calculate the absorption rate of hadrons by the medium . Considering that tens of kinds of hadrons will be discussed, the calculation of their different absorptions would be quite complicated. For simplicity, the inelastic absorption rate of a hadron by partons of type j is described as

$$\begin{aligned} j(p) &= \int_0^Z g_j(q) j_{\nu} v_{qj} j(p;q) dq \\ &= 4 \int_0^Z q^2 g_j(q) j_{\nu} j(p;q) \frac{(v+v_q)^3 j_{\nu} v_{qj}^3}{6vv_q} dq; \end{aligned} \quad (15)$$

where $v_q = q/E$ denotes the parton velocity, g_j is the parton thermal distribution at the critical temperature T_c determined by the hydrodynamic equation, and $j_{\nu} j(p;q)$ is the effective absorption cross section. Replacing $j_{\nu} j(p;q)$ by its average value j_{ν} , we obtain the total absorption rate

$$j(p) = 4 \sum_j j_{\nu} j(p) \quad (16)$$

with

$$\begin{aligned} j(p) &= \int_0^Z \frac{p_{\perp}^2 v}{1-v^2} v g_j(q) q^2 + \frac{1}{3v} g_j(q) \frac{q^4}{E_j^2} dq \\ &+ \int_0^Z \frac{p_{\perp}^2 v}{1-v^2} g_j(q) \frac{q^3}{E_j} + \frac{v^2}{3} g_j(q) q E_j dq; \end{aligned} \quad (17)$$

Taking into account the constituent quark model, the baryon cross section is set to be 1.5 times the meson cross section, $h_{bi} = 1.5h_{mi}$.

For high momentum hadrons passing cold matter, we have

$$\begin{aligned} j(p) &= \int_0^Z v g_j(q) q^2 dq + \frac{1}{3v} \int_0^Z g_j(q) \frac{q^4}{E_j^2} dq \\ &= \frac{n_j}{4} v + \frac{1}{3v} h_{vj}^2 i; \end{aligned} \quad (18)$$

where, $h_{vj}^2 i$ is a constant at given temperature and chemical potential, and n_j is the parton density. In this case, the total rate can be approximately expressed as

$$j(p) = \frac{v}{L}; \quad (19)$$

where $L = 1 = \int_0^P n_j j$ is the inelastic mean free path.

For soft hadrons in hot medium, we have

$$\begin{aligned} j(p) &= \int_0^Z v g_j(q) \frac{q^3}{E_j} dq + \frac{v^2}{3} \int_0^Z g_j(q) q E_j dq \\ &= \frac{n_j}{4} h_{vj}^2 i + \frac{v^2}{3} h_{vj}^{-1} i; \end{aligned} \quad (20)$$

Taking $h_{vj}^2 i = h_{vj}^{-1} i = 1$ for gluons and light quarks and $h_{vj}^2 i = 0.96$ and $h_{vj}^{-1} i = 1.05$ for strange quarks with mass $m_s = 95 \text{ MeV}$, the total rate becomes approximately

$$j(p) = \frac{1+v^2=3}{L}; \quad (21)$$

For the productions of color singlets, two constituents in QGP combine into a meson or an intermediate baryon state, and baryons can be described by combining different processes of $(\frac{1}{2})$, $(\frac{3}{2})$ and $(\frac{5}{2})$ intermediate baryon states [24], see Appendix A. For simplicity, we neglect those many-body channels and direct 3-quark combinations due to their small phase space.

The produced hadron density in coordinate and time space through combination of two constituents j and k at a fixed channel I can be defined as [32]

$$n_I = \int_0^Z j_{\nu} v_k j_{\nu} j(p_j) g_k(p_k) j_{\nu} j(p_k; p) d^3 p_j d^3 p_k; \quad (22)$$

where g_j and g_k are the constituent distributions, and $j_{\nu} j$ is the cross section,

$$\begin{aligned} j_{\nu} j(p_k; p) &= (2)^4 \frac{M_{Ij}^2}{4 (p_j + p_k - p)^2 m_j^2 m_k^2} \\ &= 4 (p_j + p_k - p)^2 (p^2 - m^2) (E)^2 \frac{d^4 p}{(2)^3} \end{aligned} \quad (23)$$

with the scattering matrix element M_{Ij} .

For baryon production, since a diquark is much heavier than the corresponding quark, the hadron density can be approximately expressed as [24, 33],

$$n_I = 2^3 \int_0^Z M_{Ij}^2 g_j(E_j) g_k(E_k) dE_j dE_k; \quad (24)$$

where the integrated region is restricted by the constraints

$$\begin{aligned} m_j &= E_j - 1; \\ E_j E_k &= \frac{(E_j + E_k) (m_j^2 E_k + m_k^2 E_j)}{m^2} + E_c^2; \\ E_c &= \frac{1}{2m} \frac{q}{[m^2 - (m_j + m_k)^2] [m^2 - (m_j - m_k)^2]}; \end{aligned} \quad (25)$$

Since we have assumed thermalization of quarks, gluons and diquarks, their distribution functions can be written as

$$g_j(p_j) = g_j(E_j) = \frac{j!}{(2)^3} \frac{e^{-\frac{E_j}{T_c}}}{e^{-\frac{E_j}{T_c}} - 1}; \quad (26)$$

where $j! = 3J_j (J_j + 1)$ is the degeneracy factor of spin and color degrees of freedom, and $j!$ is the reduction factor resulted from the volume effect of the bound-state or resonance-state components [31],

$$j! = [(1 - Y_0) + C_t Y_0]^{j-1} (1 - Y_0)^1;$$

with l being the number of bound states or resonant states and C_t the "transparency" of bags. For simplicity, we set $C_t = 1$.

Making summation over all the possible channels, we obtain the final hadron density

$$n = \sum_I C_I n_I; \quad (27)$$

where C_I is the weight factor of channel I and is listed in Appendix A for different channels.

To have detailed information on the produced hadrons, we need the hadron momentum distribution

$$\frac{dn_I}{4 p^2 dp} = \frac{1}{2} \frac{M_I j^Z}{pE} F(E_k) g_j(E_k) g_k(E_k) dE_k; \quad (28)$$

where F is defined as

$$F(E_j) = \frac{q \sqrt{E E_k (m^2 + m_j^2 + m_k^2) (E^2 m_k^2 + E_k^2 m^2)}}{m E_c}; \quad (29)$$

and the integrated region is restricted by the constraint

$$\begin{aligned} E_{max} &= E_k + E_{min}; \\ E_{max} &= M_{ax} f m_k; E_g; \\ E_{min} &= M_{in} f E - m_j; E + g; \\ E &= \frac{E - m^2 - m_j^2 + m_k^2 - 2m p E_c}{2m^2}; \end{aligned} \quad (30)$$

With the known produced hadron density, the gain term in the transport equation (2) can be written as

$$(\rho) = \sum_I C_I \frac{dn_I}{(4 p^2) dp}; \quad (31)$$

Note that in the calculation of loss and gain terms above, we considered only hadronization and hadron interactions with the QGP constituents. When the hadron decay in the transport process is included, it will certainly change the loss and gain terms. Its contribution to the production rate will be effectively discussed in Section IV, and the change in the absorption rate can be described by a shift [34]

$$! + -; \quad (32)$$

where Γ is the hadron decay width and γ is the Lorentz factor of the hadron.

In principle, all the particle masses are temperature and chemical potential dependent [35, 36]. For quarks and gluons at the hadronization, we can simply take $m_g = 0$, $m_u = 3 \text{ MeV}$, $m_d = 6 \text{ MeV}$ and $m_s = 95 \text{ MeV}$ [34], but for light hadrons, their masses are in principle controlled by chiral symmetry and therefore deviate from their vacuum values. To simplify calculations, we will still use their masses and decay widths in the vacuum and neglect the medium effect. As for the diquark

and qq states, their masses in the vacuum [31] are taken as $m_{qq} = 485 \text{ MeV}$, $m_{qs} = 580 \text{ MeV}$ in 0^+ channel, $m_{qq} = 725 \text{ MeV}$, $m_{qs} = 820 \text{ MeV}$, $m_{ss} = 905 \text{ MeV}$ in 1^+ channel, and $m_{qq} = 610 \text{ MeV}$, $m_{sg} = 715 \text{ MeV}$ in $\frac{1}{2}$ channel. These values are a bit smaller than the estimation in constituent quark model [37].

III. QGP EVOLUTION

We now turn to the space-time evolution of QGP. For ideal QGP, it can be described by the hydrodynamic equations,

$$\partial_T T = 0; \quad \partial_j j^i = 0; \quad (33)$$

where $T = (P + \rho) u_\mu u^\mu - P g_{\mu\nu}$ is the energy-momentum tensor of the fluid, $j^i = n_i u^\mu$ refers to the conserved charge current like baryon current and strange current, and ρ ; P ; n_i and u^μ are respectively the energy density, pressure, conserved charge density and four velocity of the fluid.

To close the hydrodynamic equations, we need the equation of state of the fluid, (P) . Since the parton fluid formed at RHIC energy is a strongly coupled QGP, we include in the equation of state the u ; d ; s quarks, gluons, and all possible qq and qg resonant states. To simplify the calculation, we assume the relation $\rho = 3P$ in the QGP stage.

From the hydrodynamic equation (33) and the equation of state, we can obtain the energy density as a function of space and time. When ρ reaches ρ_c corresponding to the critical temperature T_c for deconfinement, the expansion of the system will no longer change the temperature, and the decrease of ρ is assumed due to the splitting of the QGP fluid. Therefore, for the expansion process at fixed temperature T_c , the ratio of the energy densities ρ_c is always less than 1. Finally, when the energy density drops down to the value ρ_b for the hadronization, which is a free parameter in our calculation, the hadron emission starts and the hydrodynamic evolution of the system becomes

$$\partial_T \bar{T} = 0; \quad \partial_j \bar{j}^i = 0; \quad (34)$$

where \bar{T} and \bar{j}^i are the changes in energy-momentum tensor and conserved charge current due to the hadron emission, and they are determined by the energy loss (11) and momentum loss (12). In this way, the evolution of the decoupling hypersurface of the fluid is determined by both the hydrodynamics and the evaporation, similar to the method in FCT calculations [38, 39].

We discuss now, as an example, the spherical expansion of hydrodynamics to demonstrate the influence of evaporation on the hadronization boundary. The $1 + 1$

hydrodynamics of QGP can be written as [40],

$$\begin{aligned} \frac{\partial}{\partial t} &= \frac{2}{3} \frac{1}{v^2} v \frac{\partial}{\partial r} + 2 \frac{\partial v}{\partial r} + 2(N-1) \frac{v}{r} ; \\ \frac{\partial v}{\partial t} &= \frac{1}{3} \frac{1}{v^2} \frac{3(1-v^2)^2}{4} \frac{\partial}{\partial r} + 2v \frac{\partial v}{\partial r} \\ &\quad (N-1) \frac{v^2(1-v^2)}{r} ; \\ \frac{\partial n}{\partial t} &= v \frac{\partial n}{\partial r} + n \frac{\partial v}{\partial r} + (N-1)n \frac{v}{r} \end{aligned} \quad (35)$$

for the spherical hydrodynamic velocity v , the scaled energy-momentum quantity $\epsilon = \ln[(\epsilon + P)/(\epsilon_b + P_b)]$, and the conserved charge density $n = n_B$, where γ is the Lorentz factor of the fluid, n_B is the baryon density, and $N = 3$ is the symmetric dimension.

Similarly, we can derive the simplified 1+1 hydrodynamic equation including the feedback from the hadron evaporation. When calculated from the hydrodynamics with evaporation is less than ϵ_b , the hadronization hypersurface is determined by (35). Otherwise, the hydrodynamics with evaporation itself gives the hypersurface.

The radius R of the hadronization spherical surface, the hydrodynamic expansion velocity v on the surface, and the bulk energy of the fluid are shown as functions of time in Fig.1 for different values of shrinking velocity v_s which characterizes the effect of hadron emission on the shift of hadronization hypersurface. In the calculation, we have chosen the initial energy density distribution as a Gaussian distribution with the central value $\epsilon(r=0) = 9\epsilon_b$ and the initial expansion velocity $u(r) = v = 0.05r \text{ fm}^{-1}$. For $v_s = 0$ which means no hadron emission, the radius and the expansion velocity are fully determined by the hydrodynamic equations (35). With increasing hadron emission, the shrinking velocity increases, and the hadronization radius, the expansion velocity and the bulk energy deviate from the pure hydrodynamic solution more and more strongly. Since the hydrodynamic expansion grows with increasing time, the quantities are always controlled by the pure hydrodynamics and the emission effect can be neglected in the later stage of the fluid.

To study the space-time evolution of relativistic heavy ion collisions at RHIC energy, it is better to consider the cylindrical expansion of hydrodynamics. As is usually done, the longitudinal expansion can be decoupled from the transverse expansion and described in the Bjorken boost invariant scenario [41]. The transverse expansion is described by equation (35) with $N = 2$. As an example, we consider a central Au-Au collision at colliding energy $\sqrt{s} = 200 \text{ GeV}$. The initial condition of the collision, which is the same as in [6, 17], is determined by the nuclear geometry [42] and the corresponding nucleon-nucleon interaction. The formation time of the locally thermalized fluid is set to be $t_0 = 0.6 \text{ fm} = c$.

The hadronization radius R in the transverse plane and the corresponding expansion velocity v at R are shown

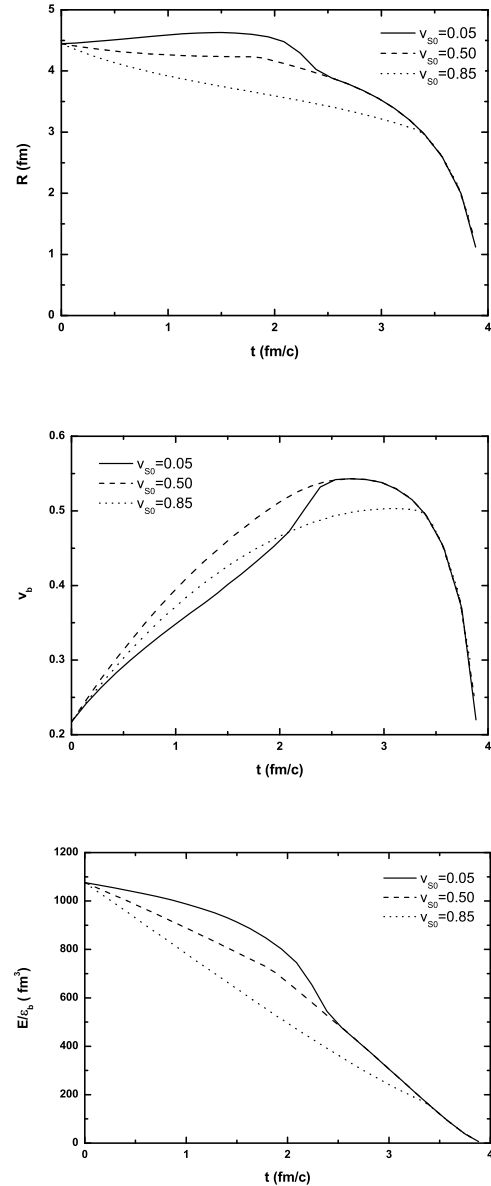


FIG. 1: The hadronization radius R , the expansion velocity v at the radius, and the bulk energy E_b scaled by the hadronization energy density ϵ_b of the QGP fluid as functions of time for several values of shrinking velocity v_s , calculated in the frame of spherical expansion.

in Fig.2. The hadronization energy density is chosen as $\epsilon_b = 0.21 \text{ GeV}/\text{fm}^3$ by fitting the RHIC data, and the shrinking velocity v_s is the maximum of its value solved from the self-consistent equations (11) and (13) for the emission energy and its value determined from the QGP hydrodynamic equation with splitting. Different from the spherical expansion where the hadron emission plays an essential role in determining the hadronization radius, the evaporation in the frame of cylindrical expansion does not change the pure hydrodynamic result considerably,

except in the very beginning period. This behavior is due to the rapid expansion in the Bjorken scenario.

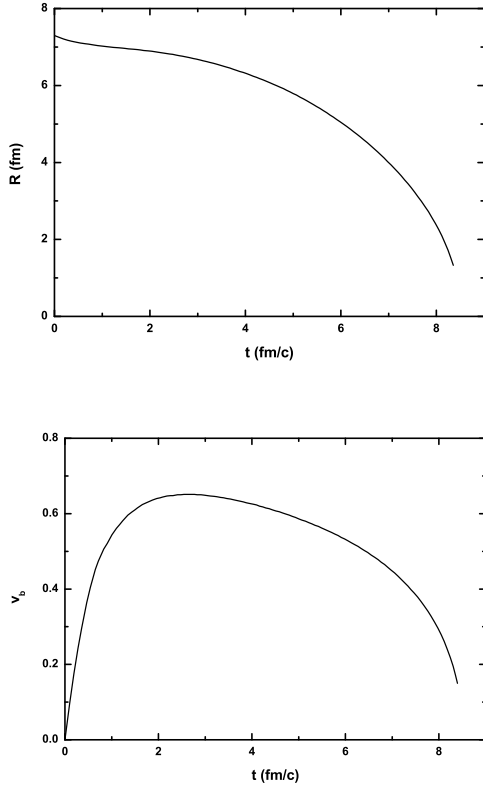


FIG. 2: The hadronization radius R and the corresponding expansion velocity v of the QGP fluid as functions of time in a central Au-Au collision with colliding energy $\sqrt{s} = 200$ GeV per pair of nucleons, calculated in the frame of cylindrical expansion.

IV. HADRON PRODUCTION AT RHIC

Now it is the time for us to apply our model with hydrodynamics for QGP evolution and transport for hadron emission to relativistic heavy ion collisions. We will calculate the spectra of soft hadrons produced in central Au-Au collisions at colliding energy $\sqrt{s_{NN}} = 200$ GeV and compare the results with experimental data at RHIC [43, 44, 45, 46, 47, 48, 49, 50, 51, 52, 53, 54, 55].

Let's first list the free parameters in the model. We choose the critical temperature $T_c = 166$ MeV which leads to the critical energy density $\epsilon_c = 1.91$ GeV/fm³. Since resonant states of qq and $q\bar{q}$ are taken into account in our equation of state for the strongly coupled QGP, the energy density is larger than the Stefan-Boltzmann limit for the ideal system of quarks and gluons, $\epsilon_c = 1.24 s_B$. The average cross section for meson-quark inelastic scattering is taken to be $\langle \sigma_{in} \rangle = 7$ mb. The ratio y_0 to describe the finite volume effect of hadrons is taken as 0.83.

From our numerical calculation, the obtained hadron spectra are not sensitive to the value of y_0 in a wide region. To minimize the free parameters, we assume that the hadrons are not thermalized at all, namely we take the relaxation time $\tau = 1$ for all hadrons. In this case, the hadron distribution is controlled only by the emission rate and medium absorption,

$$f_1(p) = \frac{f(p)}{v(p)}; \quad (36)$$

Furthermore, by fitting the PHENIX data [43] of protons and pions, we determine the energy density of the QGP fluid $\epsilon_b = 0.21$ GeV/fm³ at hadronization which corresponds to the ratio $\mu_b = \mu_c = 0.11$, the chemical potential $\mu_B = 27$ MeV at hadronization, and the meson-quark and baryon-quark coupling constants $g_M^2 = 5.11$ and $g_B^2 = 34.24$. For strange quark s , its chemical potential is $\mu_s = \mu_B = 3 \mu_s$ where μ_s is the strange chemical potential. With the above parameters, the evolution duration of the QGP fluid, calculated from the hydrodynamic equation, is about 8.4 fm/c.

The invariant yields of hadrons with type i can be calculated from the phase space integration of the hadron distribution

$$\frac{d^2 N_i}{2 p_T dp_T dy} = \frac{d}{2 p_T dp_T} \int_j^Z f_1^j(q^0) v_j^0 \cos \theta_s^0 F_D^{ji}(q;p) d^2 x dt d^3 q^0; \quad (37)$$

where F_D^{ji} stands for the decay from hadrons of type j to the hadrons of type i , q^0 is the hadron momentum in the local rest frame of the hadronization hypersurface and is related to the momentum q by a Lorentz transformation. It is necessary to note that, the decay contribution to the gain term, mentioned in the last section, can be effectively described by multiplying the decay term F_D^{ji} here by a factor

$$j_i = 1 + j_{+1;j} + j_{-1;j} j_{+2;j+1} + \dots + j_{i-1;j} \quad (38)$$

with

$$j_{+1;j} = \frac{j^-(j)}{i^+ i^-(i)}; \quad (39)$$

where we have considered the assumption of $\epsilon = 1$.

The phase space integration is done by a Monte-Carlo simulation, which partially trace the directly emitted hadrons. By counting enough events, the statistical error for $dN = dy$ caused by the random simulation is less than 0.5% - 1% for different hadrons. The statistical error for p_T distribution is, however, relatively larger, especially in very low p_T and high p_T regions. The reason is the denominator p_T in (37) for low p_T hadrons and low abundance for high p_T hadrons. In the region of $p_T = 0.3 - 4$ GeV, the statistical error is expected to be smaller than 5% for most hadrons.

The light hadron yield is dominated by decay product. For example, the number of direct pions is less than 5%

of the total final state pion abundance. Since the convergence of heavy resonance decay contribution is slow, many resonances need to be considered in our calculations. The selection of hadron types is subject to their relative production rates and branch ratios, compared with their daughter particles counted in our calculations. Mesons and baryons included in our model are listed in Table I and II. Although some of 0^+ particles, such as $f_0(600)$, $f_0(980)$ and $a_0(980)$ are often interpreted as non- $q\bar{q}$ states, they are still treated as scalar mesons in our calculations.

0	1	0^+	1^+	2^+
		a_0 980	b_1 1235	K_2 1430
K	K^* 892	f_0 600	h_1 1170	
	ρ	f_0 980	a_1 1260	
		K_0 1430	f_1 1285	
	K 1410		K_1 1270	
			K_1 1400	

TABLE I: Mesons selected in the calculations.

N					
N 938	1232	1116	1192	1317	1672
N 1440	1600	1405	1385	1530	
N 1520	1620	1520	1660	1690	
N 1535		1600	1670	1820	
		1670	1750		
		1690	1775		
		1830			

TABLE II: Baryons selected in the calculations.

The hadron spectra and relative ratios are calculated with the invariant momentum distribution (37) at $y = 0$. Since the data for exclusive protons and inclusive pions from PHENIX [43] are used to fit the parameters, the agreement between our model calculation and the data for these two kinds of particles, shown in Figs. 3, 4 and 5, looks perfect.

As only soft particles are emitted from the QGP fluid itself, the hadron spectra in high transverse momentum region are expected not to be reproduced correctly in our model. For these high p_T particles, we should consider the jet motion in QGP and its fragmentation mechanism. The effect of jets or shower partons in high p_T region is more significant for pions and protons, compared with those heavy resonances, especially multi-strange heavy resonances. The big difference between our model calculation and STAR data [45] for high p_T pions and protons is shown clearly in Figs. 6 and 7.

The transverse momentum distributions for charged kaons are shown in Fig. 8. Our model result looks higher than the experimental data. The reason is probably the lack of heavy resonances in our hadron list or the light strange quark with $m_s = 95$ MeV [34]. A heavier strange

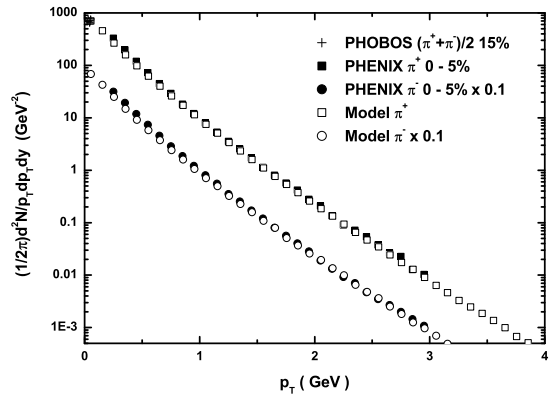


FIG. 3: The transverse momentum distributions of pions. The abundances are inclusive, and no feed-down corrections are applied. The data are from PHENIX [43] and PHOBOS [44] Collaborations.

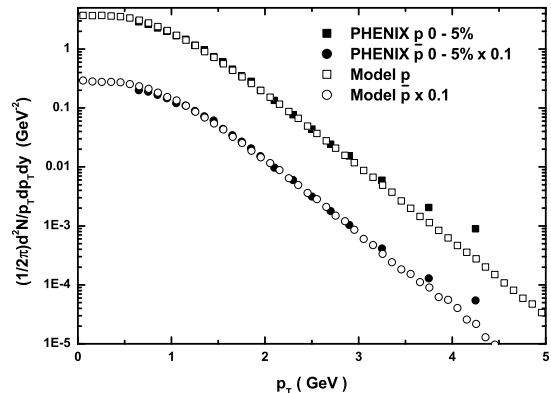


FIG. 4: The transverse momentum distributions of protons and anti-protons. The feed-down corrections from Λ are applied. The data are from PHENIX Collaboration [43].

quark can reduce the production of strange hadrons like kaons, $\Lambda(1385)$ and $\Lambda(1530)$. For $m_s = 170$ MeV, the suppression for kaons is about 5%. Another possible reason for the overestimation of kaons is the strange hadron thermalization. If we take the relaxation time $\tau = 1$ fm, the model calculation agrees well with the data.

The Λ and Σ spectra are shown in Figs. 9 and 10. The model describes well the data, but the result deviates from the data for Λ and Σ remarkably in low p_T region, especially for the positive Λ . Compared with the experimental data, a general behavior of our model calculation is the enhancement of strange mesons and suppression of strange baryons. This is probably due to the exclusion of the hadron rescattering, such as $N + K \rightarrow (\Lambda) + \dots$ or $N + K \rightarrow (\Sigma) + X$, or the treatment of diquarks. In our current frame, diquarks are thermalized like quarks and gluons and satisfy the

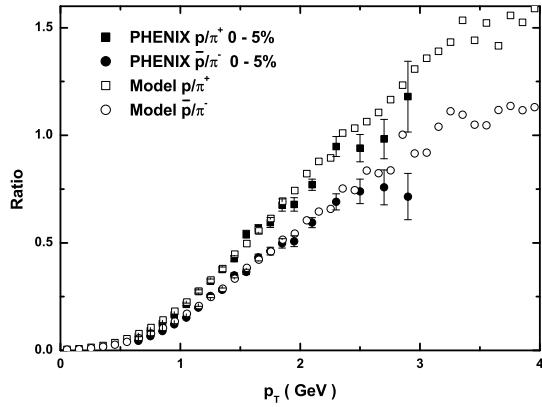


FIG. 5: The p/π^+ and p/π^- ratios as functions of transverse momentum. The data are from PHENIX Collaboration [43].

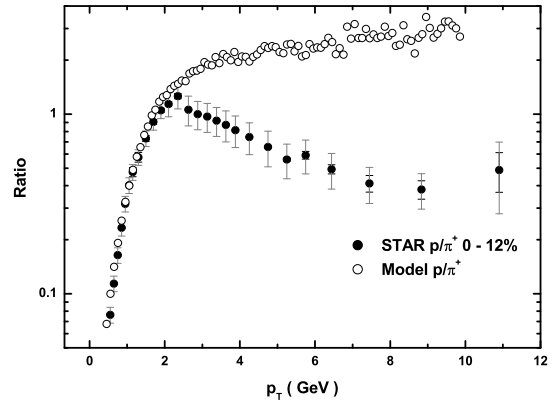


FIG. 7: The p/π^+ ratio as a function of transverse momentum. The distribution for proton is inclusive, and the decay contribution from Λ and K_S^0 to pions is removed. The data are from STAR Collaboration [45].

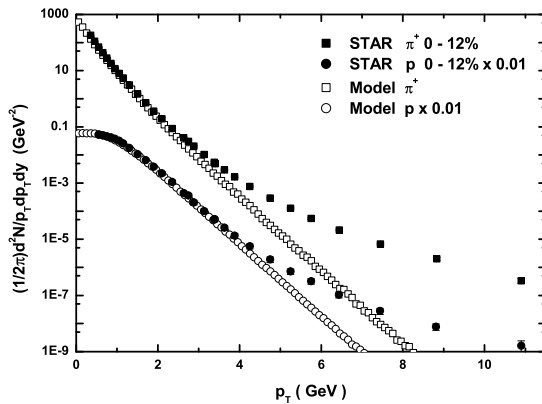


FIG. 6: The transverse momentum distributions of proton and π^+ . The distribution for proton is inclusive, and the decay contribution from Λ and K_S^0 to pions is removed. The data are from STAR Collaboration [45].

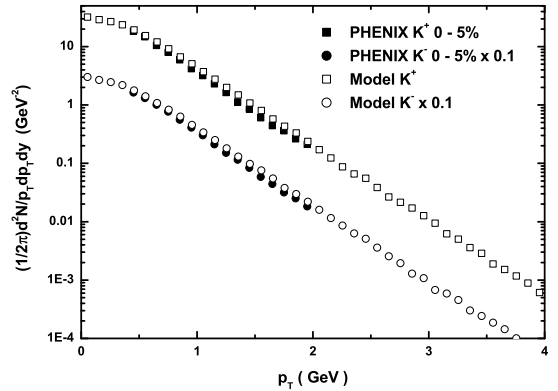


FIG. 8: The transverse momentum distributions of K^+ . The abundances are inclusive and no feed-down corrections are applied. The data are from PHENIX Collaboration [43].

Bose-Einstein distribution. Since diquarks are so heavy, it is more reasonable to describe their phase-space distribution by a transport equation, like the one for hadrons.

The transverse momentum distributions for π ; K^+ and K_S^0 and the ratio π/K_S^0 are shown in Figs. 11 and 12. Again we see clearly the theoretical enhancement for K and suppression for π . From the comparison with the STAR data, the inclusive distribution without the feed-down correction seems much better than the one shown in Fig.9. Different from the theoretical soft p/π ratio shown in Fig.7 where the ratio never decreases, the soft π/K ratio begins to drop down at about $p_T \approx 4$ GeV.

The K^+ (892) yield is shown in Fig. 13 as a function of $m_T - m_K$, where $m_T = \sqrt{p_T^2 + m_K^2}$ is the particle transverse mass. From the comparison with the STAR

data, the decay correction from the loss term (32) and the in-transport decay (ITD) loss plays an important role in the K^+ spectrum. Since the meson inelastic cross section is supposed to be 2=3 of the baryon cross section, the contribution from ITD loss for mesons would be more significant than the one for baryons. The transverse momentum distributions for π^0 and Λ are predicted in Fig. 14.

The π^0 production is shown in Fig.15. The model results are much larger than the experimental data. This is partially due to the limited hadron list in our treatment. Otherwise, the emission at the hypersurface for π^0 may not be effective. Note the fact that the STAR data [50] are about twice the PHENIX data [51], further precise measurement for π^0 is required.

The Λ (1385) distribution is shown in Fig. 16. The

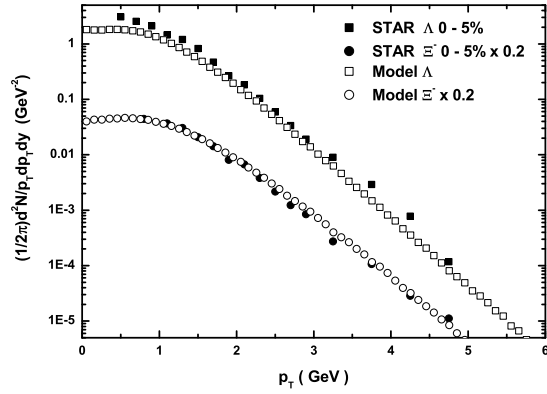


FIG. 9: The transverse momentum distributions of Λ and Ξ . The decay contribution from Σ , Σ^0 and Σ^+ is removed, but the one from Σ^0 is included. The distribution for Ξ is inclusive. All the data are from STAR Collaboration [46, 47].

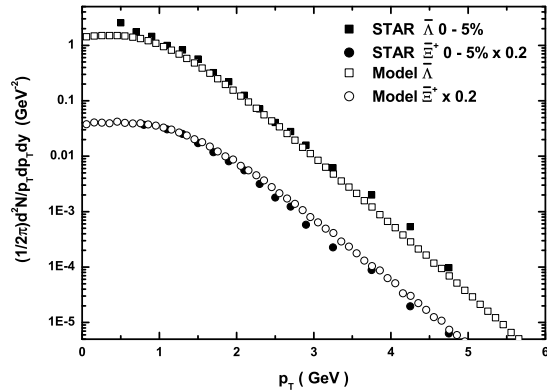


FIG. 10: The transverse momentum distributions of $\bar{\Lambda}$ and $\bar{\Xi}$. The treatment for decay contribution is the same as in Fig.9. The data are from STAR Collaboration [46, 47].

model results are much smaller than the experimental data, especially in very low p_T region. The situation here is similar to the case for Λ . The Λ or N K process which is excluded in the model may regenerate some Λ (1385) [52, 53]. As Λ (1385) can not decay to N K due to its low mass, it may become a one-way valve to deliver strange quarks from K to Λ (1385). Another possible reason for the Λ suppression is that many heavy resonances which would decay to Λ (1385) are not included in our calculation.

The transverse momentum distributions of $\Lambda(1530)$ and $\Xi(1530)$ are shown in Fig.17. For Λ , the calculated distribution is close to the data in low p_T region but deviate from the data in high p_T region. The situation is similar to Λ . This shows that either more resonances should be considered or the scenario of the hypersurface emission for these hadrons need to be corrected. From the data,

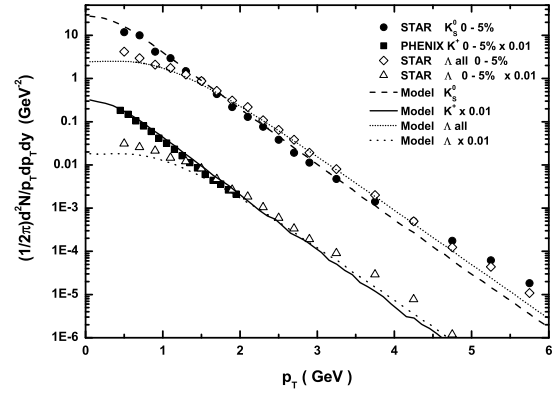


FIG. 11: The transverse momentum distributions of K_S^0 and K^+ . The distributions for K_S^0 and "all" are inclusive, and the other decay treatment is the same as in Fig.9. All the data are from STAR Collaboration [43, 46, 47, 48].

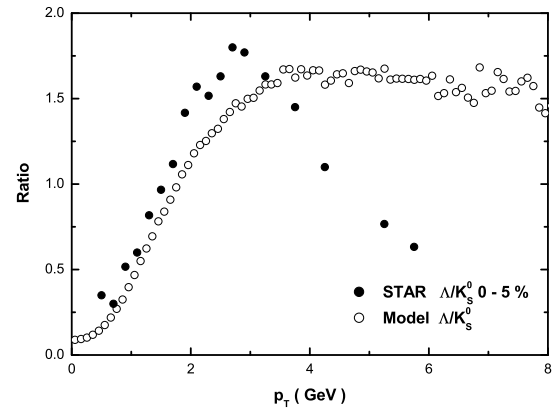


FIG. 12: The ratio Λ/K_S^0 as a function of transverse momentum. The abundances are inclusive, and no feed-down correction is applied. The data are from STAR Collaboration [48].

it looks that there are two slope parameters for Λ , like $\Lambda(1385)$ and $\Lambda(1530)$. As for $\Lambda(1530)$, the model calculation is bad at low p_T . It might be due to the fact that $\Lambda(1950)$ is not counted in our model. $\Lambda(1950)$ is a mysterious baryon. Its spin, parity and branch ratios are not clear, and it is even suggested that there might be more than one Λ at that mass [34].

The ratio of Λ to K_S^0 is presented in Fig.18 as a function of transverse momentum. As multi-strange hadrons, the jet contribution to Λ and K_S^0 is expected to be small, as we have seen in their spectra in Figs.15 and 17. Our results are similar to the ones calculated in recombination model [12].

Some of the momentum integrated ratios are listed in Table III and compared with experimental data [43, 55].

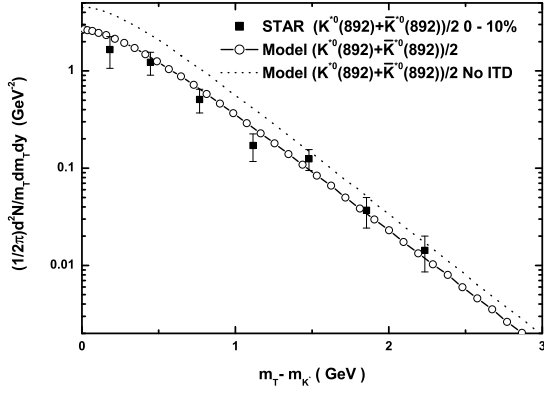


FIG. 13: The inclusive m_T distribution of $(K^0(892) + \bar{K}^0(892))/2$. The dotted line is the model calculation without considering the in-transport decay (ITD) loss correction. The data are from STAR Collaboration [49].

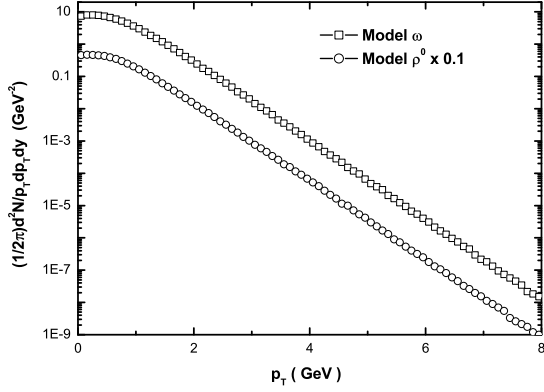


FIG. 14: The model predicted inclusive distributions of ϕ^0 and ρ^0 .

The data from [55] correspond to baryons in the p_T region of 2.4–3.6 GeV and mesons in the p_T region of 1.6–2.4 GeV. The influence of hadron decay is relatively small in these regions. The strange baryon ratios at colliding energy $\sqrt{s} = 200$ GeV [55] are very similar to the data at energy $\sqrt{s} = 130$ GeV [56, 57, 58]. Some meson and baryon ratios as functions of transverse momentum are shown in Figs. 19 and 20.

ϕ^0 and ρ^0 particles are sensitive to the hadronization mechanisms. In some string fragmentation models the ratio ϕ^0/ρ^0 is taken to be 0.35, but in thermal statistical models it is predicted to be 0.65–0.75 due to the mass difference. If the hadronization is dominated by gluon junction or coalescence, the ratio is about 1. In our case, the hadronization mechanism is similar to the coalescence or recombination, but the ratio is a little larger than 1 [24, 33]. The reason is that ϕ^0 contains an important component $B_{\frac{1}{2}}(A_{ud};s)$, described in Appendix

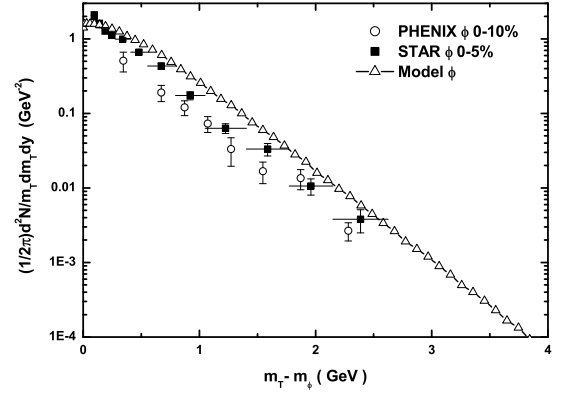


FIG. 15: The inclusive m_T distribution of $\phi(1020)$. The x error bar is used here to show the m_T bin size. The data are from STAR [50] and PHENIX [51] Collaborations.

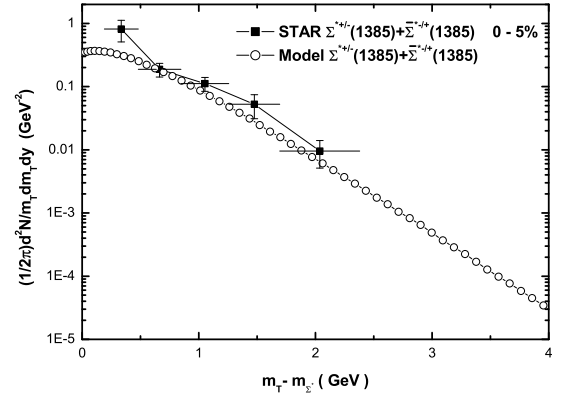


FIG. 16: The inclusive m_T distribution of $(\Sigma^+(1385) + \Sigma^-(1385))/2$. The data are from STAR Collaboration [52].

A , but this term does not exist for ϕ^0 with isospin zero.

With the selected parameters, the direct ratio ϕ^0/ρ^0 is 1.181. Considering the decay contributions from heavy baryons or resonances, it decreases to 0.636. The transverse momentum distributions of direct ϕ^0 and ρ^0 , inclusive ϕ^0 , and exclusive without ϕ^0 decay contribution are shown in Fig. 21. The transverse momentum dependence of the ratio ϕ^0/ρ^0 with and without considering the decay contribution are shown in Fig. 22.

Since it is difficult to extract ϕ^0 through electromagnetic decay, ρ^0 may be easier to be determined if ϕ^0 is well measured. Their production is supposed to be similar to ϕ^0 . The expected ρ^+ production is shown in Fig. 23.

$(1405)0(\frac{1}{2}^-)$ and $(1520)0(\frac{3}{2}^-)$ are regarded as singlet states. It is not easy to determine their wave functions in quark-diquark model, and it is hard to distinguish them from the states $(L=1;S=\frac{3}{2}^-)$ and $(L=$

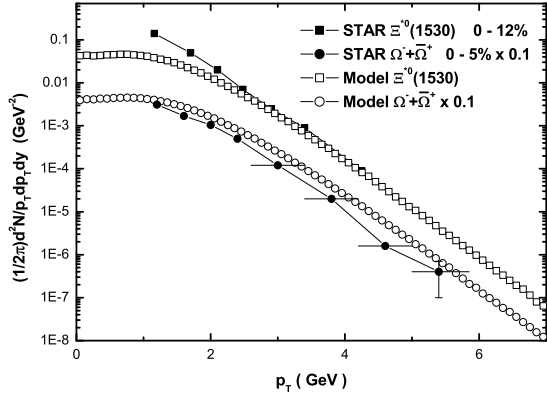


FIG. 17: The inclusive transverse momentum distributions of $\Xi^0(1530)$ and $\Omega^- + \bar{\Omega}^+$. The data are from STAR Collaboration [46, 47, 53].

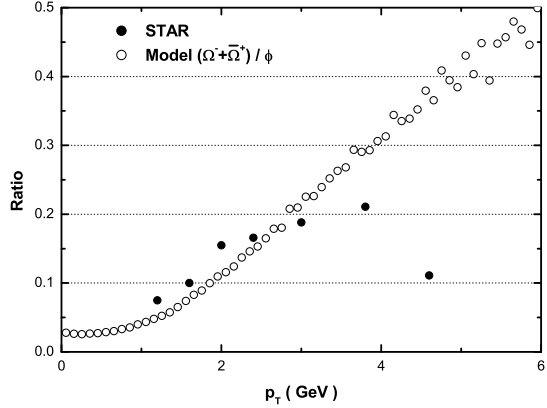


FIG. 18: The inclusive ratio $(\Omega^- + \bar{\Omega}^+) =$ as a function of transverse momentum. The data are from STAR Collaboration [54].

$1; S = \frac{1}{2}$). A rough estimation of (1405) and (1520) production is shown in Fig. 24, where (1405) and (1520) are, respectively, supposed to be $(L = 1; S = \frac{1}{2})$ octet and $(L = 1; S = \frac{3}{2})$ octet. The details on their wave function construction is given in Appendix A.

At the end of the discussion on hadron spectra, we consider the ratio $\bar{p}/p =$. When diquarks are considered as constituents of the strongly coupled QGP, the strange chemical potential of the system will increase due to the negative strange numbers of diquarks us and ds . In our calculations, the strange chemical potential $\mu_s = 9.35$ MeV is extracted from the strange charge conservation. In this case, the strange quark and diquark ss will carry negative chemical potentials, $\mu_s = 0.35$ MeV and $\mu_{ss} = 0.7$ MeV [33]. The string fragmentation model [59] with diquarks gives similar result. However, the ratio in the

P particles	Model	Exp		
$\bar{p} = +$ (in)	1.006	0.984	0.004	0.057 [43]
$\bar{p} = +$ (ex)	0.999	1.01	0.02	[55]
$K^- = K^+$	0.915	0.933	0.007	0.054 [43]
		0.96	0.03	[55]
$p = p$ (ex)	0.748	0.731	0.011	0.062 [43]
$p = p$ (in)	0.783	0.747	0.007	0.046 [43]
		0.77	0.05	[55]
$\bar{p} =$	0.844	0.72	0.024	[55]
$\bar{p} = +$	0.907	0.82	0.05	[55]
$\bar{p} =$	1.011	1.01	0.08	[55]
$K^+ = +$	0.203	0.171	0.001	0.010 [43]
$K^- =$	0.184	0.162	0.001	0.010 [43]
$p_{ex} = +$	0.0645	0.064	0.001	0.003 [43]
$p = +$ (in)	0.102	0.099	0.001	0.006 [43]
$p_{ex} =$	0.0479	0.047	0.001	0.002 [43]
$p =$ (in)	0.0797	0.075	0.001	0.004 [43]

TABLE III: Some momentum integrated hadron ratios compared with RHIC data [43, 55]. The statistical errors in the model calculations are up to 5%.

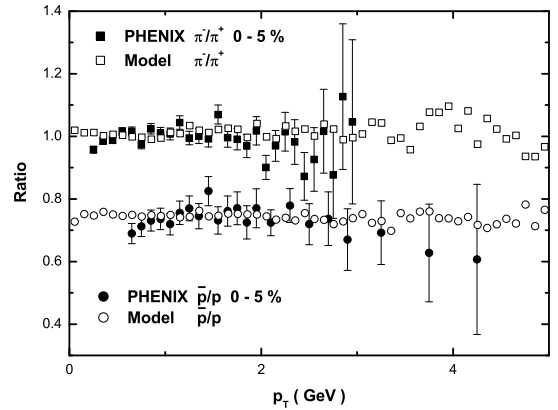


FIG. 19: The inclusive \bar{p}/p and exclusive $p = p$ ratios as functions of transverse momentum. The data are from PHENIX Collaboration [43].

calculation without diquarks is $\bar{p} = + = 1$ [3, 60].

As shown in Table III, the ratio $\bar{p} = + = 1.011$ is consistent with the STAR measurement [55]. While the diquarks are supposed in thermal equilibrium in our model, and the current data are still with large statistical and systematic errors, the qualitative conclusion of $\bar{p} = + > 1$ is supposed not to be changed.

As pointed above, the thermalization of final state hadrons are omitted in all of the calculations. Considering the interactions which are not inserted in our treatments, some of the dominant hadrons would be partially thermalized effectively. Comparing with the RHIC data, π, K, p and \bar{p} may be well thermalized, while the heavy baryons may be not.

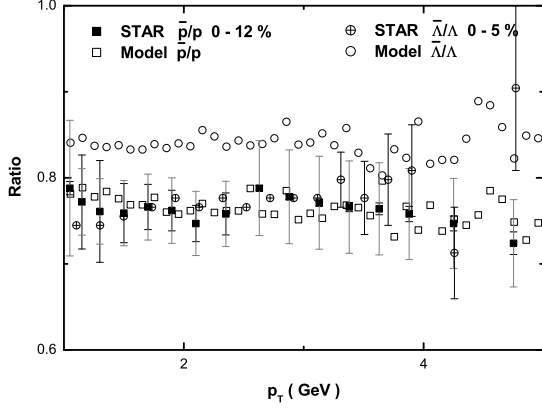


FIG. 20: The inclusive p/p and Λ/Λ ratios as functions of transverse momentum. The data are from STAR Collaboration [45, 48].

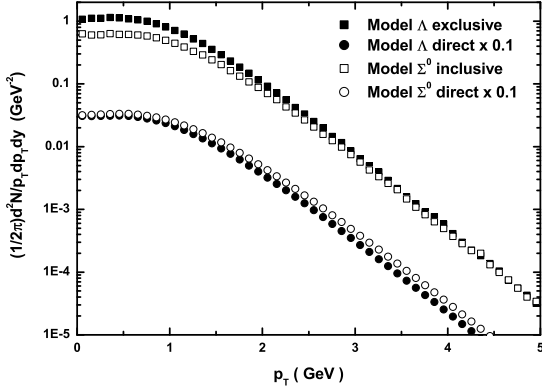


FIG. 21: The model predicted transverse momentum distributions of direct Σ^0 and Λ , inclusive Σ^0 , and exclusive Σ^0 . The decay contribution from Σ^0 , Λ , Σ^0 and Λ to the exclusive Σ^0 are removed.

V. SUMMARY

We have developed a phenomenological model to describe hadron production in relativistic heavy ion collisions. In our model, the QGP evolution and hadron transport are coupled to each other in a self-consistent way. The strongly coupled QGP, including not only gluons and quarks but also their resonant states like diquarks, is described by ideal hydrodynamics, and the hadrons emitted from the QGP satisfy transport equations with loss and gain terms. The hadron decay is effectively reflected in the medium absorption and hadron spectra. Due to the feedback of the hadron emission, the hadronization hypersurface of the parton fluid shrinks with a constant velocity. The splitting of the fluid due to its fast expansion in the later stage and the hadron emis-

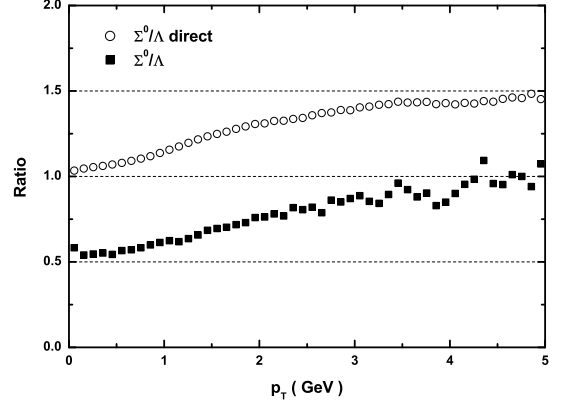


FIG. 22: The ratio Σ^0/Λ as a function of transverse momentum, with and without considering decay contribution.

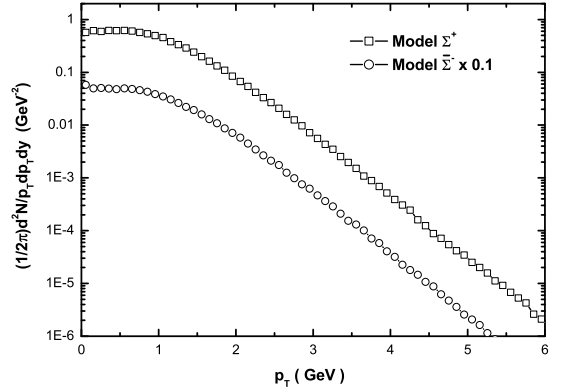


FIG. 23: The expected transverse momentum distributions of direct Σ^+ and Σ^- . No feed-down correction is applied.

sion is also effectively considered, by introducing a ratio of the volume of the QGP droplets to the whole volume of the system. We applied our model to calculate the final state hadron spectra in heavy ion collisions. From the comparison with the RHIC data, most of the hadron spectra and hadron ratios can be reasonably described in our model.

The model deserves further improvement in future studies. Unlike the quarks and gluons, the diquarks in QGP are resonant states and they should behave differently. Since mesons are described by transport equations in our model, the thermalization of diquarks are in principle not self-consistent. Different types of hadrons will have different thermalization time. Light hadrons are easy but heavy hadrons are difficult to get thermalized. In our current treatment, the relaxation time in the hadron transport equations is taken to be infinity, and therefore, no hadron can be thermalized in the whole evolution. The treatment of the QGP fluid splitting is also

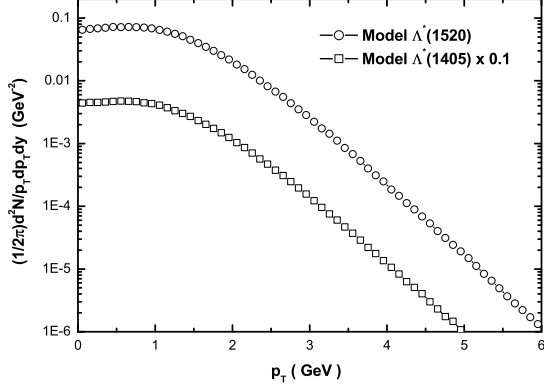


FIG. 24: The model calculated transverse momentum distributions of (1405) and (1520), with the wave functions listed in Appendix A. No feed-down correction is applied.

too simple in our model. When the model is improved, it can be used to calculate more hadron distributions like the elliptic flow [61, 62], which is considered to be sensitive to the thermalization of the system in the early stage.

Acknowledgements: We are grateful to Wojciech Broniowski, Huanzhong Huang, Rudolph C. Hwa, Yuxin Liu, Sevil Salur, Qubing Xie, Nu Xu and Weining Zhang for useful discussions. The work is supported in part by the grants No. NSFC 10547001 and 10425810.

APPENDIX A: REWRITING THE BARYON WAVE FUNCTIONS

The SU(6) baryon wave functions can be rewritten in the quark-diquark model [63, 64]. The $(\frac{1}{2})^+$ and $(\frac{3}{2})^+$ s-wave intermediate baryon states are introduced as

$$\begin{aligned}
 B_{\frac{1}{2};+\frac{1}{2}}(A;q) &= \frac{1}{\sqrt{3}} h p_{-}^{-} 2A_{+} q^{\#} A_0 q^{\#i}; \\
 B_{\frac{1}{2};+\frac{1}{2}}(S;q) &= S q^{\#i}; \\
 B_{\frac{3}{2};+\frac{3}{2}}(A;q) &= A_{+} q^{\#i}; \\
 B_{\frac{3}{2};+\frac{1}{2}}(A;q) &= \frac{1}{\sqrt{3}} h A_{+} q^{\#} + \frac{p_{-}^{-}}{2} A_0 q^{\#i}; \quad (A1)
 \end{aligned}$$

where S and A represent a scalar and an axial-vector diquark state, respectively. The nal baryon states can be expressed in terms of certain combinations of these intermediate baryon states [24, 33]. The wave functions

are expressed as

$$\begin{aligned}
 p_i &= \frac{1}{\sqrt{3}} h B_{\frac{1}{2}}(A_{uu};d) \frac{r}{2} B_{\frac{1}{2}}(A_{ud};u) \\
 &\quad + \frac{r}{2} B_{\frac{1}{2}}(S_{ud};u); \\
 n_i &= \frac{1}{\sqrt{3}} h B_{\frac{1}{2}}(A_{dd};u) + \frac{r}{2} B_{\frac{1}{2}}(A_{ud};d) \\
 &\quad + \frac{r}{2} B_{\frac{1}{2}}(S_{ud};d); \\
 j_i &= \frac{1}{\sqrt{3}} h r \frac{r}{4} B_{\frac{1}{2}}(A_{us};d) \frac{r}{4} B_{\frac{1}{2}}(A_{ds};u) \\
 &\quad + \frac{r}{4} B_{\frac{1}{2}}(S_{us};d) \frac{r}{4} B_{\frac{1}{2}}(S_{ds};u) \\
 &\quad + B_{\frac{1}{2}}(S_{ud};s); \\
 j^0_i &= \frac{1}{\sqrt{3}} h B_{\frac{1}{2}}(A_{ud};s) \frac{r}{4} B_{\frac{1}{2}}(A_{us};d) \\
 &\quad + \frac{r}{4} B_{\frac{1}{2}}(A_{ds};u) + \frac{r}{4} B_{\frac{1}{2}}(S_{us};d) \\
 &\quad + \frac{r}{4} B_{\frac{1}{2}}(S_{ds};u); \\
 j^+_i &= \frac{1}{\sqrt{3}} h B_{\frac{1}{2}}(A_{uu};s) \frac{r}{2} B_{\frac{1}{2}}(A_{us};u) \\
 &\quad + \frac{r}{2} B_{\frac{1}{2}}(S_{us};u); \\
 j^-_i &= \frac{1}{\sqrt{3}} h B_{\frac{1}{2}}(A_{dd};s) \frac{r}{2} B_{\frac{1}{2}}(A_{ds};d) \\
 &\quad + \frac{r}{2} B_{\frac{1}{2}}(S_{ds};d); \\
 j^0^0_i &= \frac{1}{\sqrt{3}} h B_{\frac{1}{2}}(A_{ss};u) + \frac{r}{2} B_{\frac{1}{2}}(A_{us};s) \\
 &\quad + \frac{r}{2} B_{\frac{1}{2}}(S_{us};s); \\
 j^-_i &= \frac{1}{\sqrt{3}} h B_{\frac{1}{2}}(A_{ss};d) + \frac{r}{2} B_{\frac{1}{2}}(A_{ds};s) \\
 &\quad + \frac{r}{2} B_{\frac{1}{2}}(S_{ds};s) \quad (A2)
 \end{aligned}$$

for the SU (3) octet baryons, and

$$\begin{aligned}
j^{++}i &= B_{\frac{3}{2}}(A_{uu};u); \\
j^{+}i &= \frac{1}{\sqrt{3}} B_{\frac{3}{2}}(A_{uu};d) + \frac{p_{-}}{2B_{\frac{3}{2}}}(A_{ud};u); \\
j^{0}i &= \frac{1}{\sqrt{3}} B_{\frac{3}{2}}(A_{dd};u) + \frac{p_{-}}{2B_{\frac{3}{2}}}(A_{ud};d); \\
j^{-}i &= B_{\frac{3}{2}}(A_{dd};d); \\
j^{+}i &= \frac{1}{\sqrt{3}} B_{\frac{3}{2}}(A_{uu};s) + \frac{p_{-}}{2B_{\frac{3}{2}}}(A_{us};u); \\
j^{0}i &= \frac{1}{\sqrt{3}} B_{\frac{3}{2}}(A_{us};d) + B_{\frac{3}{2}}(A_{ds};u) + B_{\frac{3}{2}}(A_{ud};s); \\
j^{-}i &= \frac{1}{\sqrt{3}} B_{\frac{3}{2}}(A_{dd};s) + \frac{p_{-}}{2B_{\frac{3}{2}}}(A_{ds};d); \\
j^{0}i &= \frac{1}{\sqrt{3}} B_{\frac{3}{2}}(A_{ss};u) + \frac{p_{-}}{2B_{\frac{3}{2}}}(A_{us};s); \\
j^{-}i &= \frac{1}{\sqrt{3}} B_{\frac{3}{2}}(A_{ss};d) + \frac{p_{-}}{2B_{\frac{3}{2}}}(A_{ds};s); \\
j^{-}i &= B_{\frac{3}{2}}(A_{ss};s) \tag{A 3}
\end{aligned}$$

for the decuplet baryons. From these expressions, we can get the factor C_I in Eqs. (27) and (31) to complete the production rate.

There might be other orthogonal baryon states. From the Tables of Particle Physics [34], $N(1440) \frac{1}{2}(\frac{1}{2}^{+})$ and $N(1710) \frac{1}{2}(\frac{1}{2}^{+})$ are conjectured to be the orthogonal states of p and n . Other possible orthogonal states are $(1600) 0(\frac{1}{2}^{+})$, $(1810) 0(\frac{1}{2}^{+})$, $(1660) 1(\frac{1}{2}^{+})$ and $(1880) 1(\frac{1}{2}^{+})$ of Σ and Λ , $N(1720) \frac{1}{2}(\frac{3}{2}^{+})$ of Σ^{+} and Σ^{0} , $(1890) 0(\frac{3}{2}^{+})$ and $(1840) 1(\frac{3}{2}^{+})$ of $\Sigma(1385)$, and some unknown orthogonal states of Λ and $\Sigma(1530)$. There are 24 such particles which belong to two $(\frac{1}{2})^{+}$ octets and a $(\frac{3}{2})^{+}$ octet.

The wave functions of the orthogonal baryon states in $(\frac{3}{2})^{+}$ decuplet can be determined. For example,

$$\begin{aligned}
j_{\Sigma=\frac{3}{2}}^{f8g} &= \frac{1}{\sqrt{2}} B_{\frac{3}{2}}(A_{us};d) - B_{\frac{3}{2}}(A_{ds};u); \\
j_{\Sigma=\frac{3}{2}}^{0f8g} &= \frac{1}{\sqrt{6}} B_{\frac{3}{2}}(A_{us};d) + B_{\frac{3}{2}}(A_{ds};u) - 2B_{\frac{3}{2}}(A_{ud};s);
\end{aligned} \tag{A 4}$$

There are two orthogonal baryon states in $(\frac{1}{2})^{+}$ octet. Their wave functions are not unique. Considering that the first octet state is the mixed state of Aq and Sq , a most possible assumption is that the second octet state should be the corresponding mixed state, and the third one contains no mixing. Therefore, we have

$$\begin{aligned}
j_{\Sigma=\frac{1}{2}}^{f8g} &= \frac{1}{\sqrt{3}} B_{\frac{1}{2}}(A_{uu};d) - \frac{r}{2} B_{\frac{1}{2}}(A_{ud};u) \\
&\quad + \frac{r}{3} B_{\frac{1}{2}}(S_{ud};u); \\
j_{\Sigma=\frac{1}{2}}^{0f8g} &= \frac{1}{\sqrt{3}} B_{\frac{1}{2}}(A_{uu};d) + \frac{p_{-}}{2B_{\frac{1}{2}}}(A_{ud};u);
\end{aligned} \tag{A 5}$$

where, N_2^{+} corresponds to $N(1440)^{+}$ and N_3^{+} to $N(1710)^{+}$. The other orthogonal baryon wave functions with positive parity are similar.

The wave functions of some of the $(\frac{1}{2})^{-}$ and $(\frac{3}{2})^{-}$ resonances are not clear. It is hard to distinguish a $(\frac{1}{2})^{-}$ or a $(\frac{3}{2})^{-}$ state from the two candidates ($L=1; S=\frac{1}{2}$) and ($L=1; S=\frac{3}{2}$). For simplicity, all $(\frac{1}{2})^{-}$ baryons, except $\Lambda(1520)$, are regarded as $S=\frac{1}{2}$ octet states and all $(\frac{3}{2})^{-}$ baryons are regarded as $S=\frac{3}{2}$ octet or decuplet states.

$\Lambda(1405) 0(\frac{1}{2}^{-})$ and $\Lambda(1520) 0(\frac{3}{2}^{-})$ are regarded as singlet states [34]. The quark-diquark wave functions of them are unknown. Approximately, their wave functions are written as $S=\frac{1}{2}$ octet and $S=\frac{3}{2}$ octet.

APPENDIX B: EFFECTIVE LAGRANGIAN AND MATRIX ELEMENTS OF PRODUCTION CROSS SECTION

In calculating the hadron production rate, only low-order interactions are considered. As there are not enough data to determine the coupling modes and constants, we choose only some of the most simple coupling channels. To further reduce the number of parameters, we use two universal coupling constants g_M for meson interactions with two quarks and g_B for baryon interactions with a quark and a diquark. The meson sector of the effective Lagrangian density is listed in Tab. IV for different meson. The influence of P-wave and D-wave is neglected.

Meson	Leff	$\mathcal{M}_{spin J}$
0	$ig_M q_1 \bar{q}_2$	$\frac{g_M^2}{2} [m_M^2 - (m_{q1} - m_{q2})^2]$
0^+	$ig_M q_1 \bar{q}_2$	$\frac{g_M^2}{2} [m_M^2 - (m_{q1} + m_{q2})^2]$
1	$ig_M q_1 \bar{q}_2$	$\frac{g_M^2}{2} [m_M^2 - (m_{q1} - m_{q2})^2] \left[\frac{(m_{q1} + m_{q2})^2}{m_M^2} + 2 \right]$
1^+	$ig_M q_1 \bar{q}_2$	$\frac{g_M^2}{2} [m_M^2 - (m_{q1} + m_{q2})^2] \left[\frac{(m_{q1} - m_{q2})^2}{m_M^2} + 2 \right]$
2^+	$ig_M q_1 \bar{q}_2$	$\frac{3g_M^2}{10} [m_M^2 - (m_{q1} + m_{q2})^2]$

TABLE IV: The effective interactions and the corresponding scattering matrix elements $\mathcal{M}_{spin J} = \mathcal{M}_{J=3}$ for different mesons.

For the baryon sector of the effective Lagrangian density, we take

$$\begin{aligned}
L_{qSB} &= ig_B \bar{q} B qS; \\
L_{qAB1} &= ig_B \bar{q} B \bar{q} A; \\
\mathcal{M}_B^P &= g_B^2 (m_B + m_q)^2 - m_S^2; \\
\mathcal{M}_A^P &= \frac{g_B^2}{3} (m_B + m_q)^2 - m_A^2 - \frac{(m_B - m_q)^2}{m_A^2} + 2
\end{aligned} \tag{B 1}$$

for the baryons with $J^P = \frac{1}{2}^{+}$, $L=0$ and $S=\frac{1}{2}$. Note that the scattering matrix elements here are equivalent to the expressions in [33].

For $J^P = \frac{1}{2}^-$ [65], $L = 1$ and $S = \frac{1}{2}$, we use

$$\begin{aligned} L_{qSB} &= \frac{ig_B}{m_B + m_q} B_{5q@S}; & (B2) \\ L_{qAB1} &= \frac{ig_B}{2m_A} B_{q@A}; \\ \mathcal{M}_{\frac{1}{2}^-} &= g_B^2 (m_B - m_q)^2 m_S^2; \\ \mathcal{M}_{\frac{1}{2}^+} &= \frac{g_B^2}{6} (m_B - m_q)^2 m_A^2 \frac{(m_B + m_q)^2}{m_A^2} + \frac{1}{2} \end{aligned}$$

with the definition $\mathcal{M} = i[\dots]$. The expression of L_{qSB} here gives the same result as the direct coupling [66]. For $J^P = \frac{1}{2}^-$, $L = 1$ and $S = \frac{3}{2}$, the scattering matrix elements are supposed to be the same.

We choose

$$\begin{aligned} L_{qAB} &= ig_B B_{5qA}; \\ \mathcal{M}_{\frac{1}{2}^-} &= \frac{g_B^2}{18} (m_B - m_q)^2 m_A^2 \frac{(m_B^2 + m_A^2 - m_q^2)^2}{m_B^2 m_A^2} + 8 & (B3) \end{aligned}$$

for $J^P = \frac{3}{2}^+$ [67], $L = 0$ and $S = \frac{3}{2}$, and

$$\begin{aligned} L_{qSB} &= \frac{ig_B}{m_S} B_{5q@S}; \\ \mathcal{M}_{\frac{3}{2}^+} &= \frac{g_B^2}{6} (m_B - m_q)^2 m_S^2 \frac{(m_B^2 + m_S^2 - m_q^2)^2}{m_B^2 m_S^2} + 4 & (B4) \end{aligned}$$

for $J^P = \frac{3}{2}^-$, $L = 1$ and $S = \frac{1}{2}$. For the axial-vector

couplings, the matrix element is replaced by

$$\mathcal{M}_{\frac{1}{2}^-} = \frac{g_B^2}{18} (m_B + m_q)^2 m_A^2 \frac{(m_B^2 + m_A^2 - m_q^2)^2}{m_B^2 m_A^2} + 8; & (B5)$$

and the expression for $J^P = \frac{3}{2}^-$, $L = 1$ and $S = \frac{3}{2}$ is the same.

We employ

$$\begin{aligned} L_{qAB} &= \frac{ig_B}{m_A} B_{q@A}; \\ \mathcal{M}_{\frac{1}{2}^-} &= \frac{g_B^2}{48} (m_B + m_q)^2 m_A^2 \frac{(m_B^2 + m_A^2 - m_q^2)^2}{m_B^2 m_A^2} + 5.6 & (B6) \end{aligned}$$

for $J^P = \frac{5}{2}^-$, $L = 1$ and $S = \frac{3}{2}$, where the expression of the spin- $\frac{5}{2}$ projector can be found in [68], and

$$\begin{aligned} L_{qSB} &= \frac{ig_B}{m_S} B_{q@S}; \\ \mathcal{M}_{\frac{5}{2}^-} &= \frac{g_B^2}{16} (m_B + m_q)^2 m_S^2 \frac{(m_B^2 + m_S^2 - m_q^2)^2}{m_B^2 m_S^2} + 4 & (B7) \end{aligned}$$

for $J^P = \frac{5}{2}^+$, $L = 2$ and $S = \frac{1}{2}$.

-
- [1] U. W. Heinz, Nucl. Phys. A 685, 414-431 (2001), hep-ph/0009170
[2] J. Stachel, Nucl. Phys. A 654, 119c-135c (1999), nucl-ex/9903007.
[3] J. Rafelski and J. Letessier, Phys. Lett. B 469, 12 (1999). nucl-th/9908024.
[4] P. Huovinen, Nucl. Phys. A 761, 296-312 (2005), nucl-th/0505036.
[5] G. E. Brown and M. Rho, Phys. Rev. Lett. 66, 2720-2723 (1991); G. E. Brown et al., nucl-th/0608023.
[6] P. F. Kolb and U. W. Heinz, Invited review for 'Quark Gluon Plasma 3', Editors: R. C. Hwa and X. N. Wang, World Scientific, Singapore, nucl-th/0305084.
[7] W. Florkowski, W. Broniowski and A. Baran, J. Phys. G 31, S1087-S1090 (2005), nucl-th/0412077.
[8] C. Nonaka and S. A. Bass, nucl-th/0607018.
[9] T. S. Biro and J. Zimanyi, Phys. Lett. B 113, 6 (1982); Nucl. Phys. A 395, 525 (1983);
[10] T. S. Biro, P. Levai and J. Zimanyi, J. Phys. G 28, 1561-1566 (2002), hep-ph/0112137.
[11] R. J. Fries, J. Phys. G 30, S853-S860 (2004), nucl-th/0403036;
[12] R. C. Hwa and C. B. Yang, nucl-th/0602024.
[13] M. Gyulassy, P. Levai and I. Vitev, Phys. Rev. Lett. 85, 5535-5538 (2000), nucl-th/0005032; M. Gyulassy, P. Levai and I. Vitev, Nucl. Phys. B 594, 371-419 (2001), nucl-th/0006010.
[14] Q. Wang and X. N. Wang, Phys. Rev. C 71, 014903 (2005), nucl-th/0410049.
[15] L. G. Moretto et al., Phys. Rev. Lett. 94, 202701 (2005), nucl-th/0412070.
[16] J. Adams et al., the STAR Collaboration, Phys. Rev. C 71, 044906 (2005), nucl-ex/0411036.
[17] P. F. Kolb and R. Rapp, Phys. Rev. C 67, 044903 (2003), hep-ph/0210222.
[18] J. Rafelski and J. Letessier, Eur. Phys. J. A 29, 107-111 (2006), nucl-th/0511016.
[19] H. Stoecker et al., Phys. Lett. B 95, 192-197 (1980).
[20] G. Bertsch et al., Phys. Rev. D 37, 1202-1209 (1988).
[21] W. H. Barz, B. L. Friman, J. Kroll and H. Schulz, Phys. Lett. B 242, 328-333 (1990).
[22] I. Arsene et al., Nucl. Phys. A 757, 1 (2005); B. B. Back

- et al, Nucl. Phys. A 757, 28 (2005); J. Adams et al, Nucl. Phys. A 757, 102 (2005); K. Adcox et al, Nucl. Phys. A 757, 184 (2005).
- [23] D. Teaney, J. Lauret and E. V. Shuryak, Phys. Rev. Lett. 86, 4783-4786 (2001); P. F. Kolb, P. Huovinen, U. Heinz and H. Heiseberg, Phys. Lett. B 500, 232-240 (2001).
- [24] H. Miao, Z. B. Ma and C. S. Gao, J. Phys. G 29, 2187-2192 (2003), hep-ph/0303164.
- [25] E. V. Shuryak and I. Zahed, Phys. Rev. D 70, 054507 (2004), hep-ph/0403127.
- [26] M. Huang, P. F. Zhuang and W. Q. Chao, Phys. Rev. D 67, 065015 (2003), hep-ph/0207008.
- [27] S. K. Kam, hep-ph/0510239.
- [28] S. Calogero, J. Math. Phys. 45, 4042-4052 (2004), math-ph/0404043
- [29] L. Yan, P. F. Zhuang and N. Xu, Phys. Rev. Lett. 97, 232301 (2006), nucl-th/0608010.
- [30] J. W. Clark, J. Cleymans and J. Rafelski, Phys. Rev. C 33, 703 (1986).
- [31] H. Miao, C. S. Gao and P. F. Zhuang, Commun. Theor. Phys. 46, 1040-1046 (2006), hep-ph/0511245.
- [32] C. S. Gao, in JingShin Theoretical Physics Symposium in Honor of Professor Ta-You Wu, edited by J. P. Hsu and L. Hsu, (World Scientific, 1998) 362.
- [33] H. Miao and C. S. Gao, J. Phys. G 31, 179-184 (2005), hep-ph/0404037.
- [34] W. M. Yao et al, (Particle Data Group), J. Phys. G 33, 1 (2006);
- [35] Z. Fodor and S. Katz, JHEP 0203, 014 (2002), hep-lat/0106002.
- [36] F. Karsch, Nucl. Phys. (Proc Suppl) 83-84, 14 (2000).
- [37] D. B. Lichtenberg, W. Namgung, J. G. Wills and E. Predazzi, Z. Phys. C 19, 19 (1983); D. B. Lichtenberg, R. Roncaglia and E. Predazzi, hep-ph/9611428.
- [38] J. P. Boris, D. L. Book, J. Comp. Phys. 11, 38 (1973); J. P. Boris, D. L. Book, and K. Hain, J. Comp. Phys. 18, 248 (1995).
- [39] D. H. Rischke, S. Bernard, and J. A. Marnuhn, Nucl. Phys. A 595, 346 (1995); D. H. Rischke, Y. Pursun, and J. A. Marnuhn, Nucl. Phys. A 595, 383 (1995).
- [40] H. Miao, Z. B. Ma and C. S. Gao, Commun. Theor. Phys. 38, 698-702 (2002), hep-ph/0303134.
- [41] J. D. Bjorken, Phys. Rev. D 27, 140-151 (1983).
- [42] A. Bialas, M. Bleszynski and W. Czyz, Nucl. Phys. B 111, 461 (1976).
- [43] S. S. Adler et al, the PHENIX Collaboration, Phys. Rev. C 69, 034909 (2004), nucl-ex/0307022.
- [44] B. B. Back et al, the PHOBOS Collaboration, Phys. Rev. C 70, 051901(R) (2004), nucl-ex/0401006.
- [45] B. I. Abelev et al, the STAR Collaboration, Phys. Rev. Lett. 97, 152301 (2006), nucl-ex/0606003.
- [46] M. Estienne (for the STAR Collaboration), J. Phys. G 31, S873-S880 (2005), nucl-ex/0412041.
- [47] J. Adams et al, the STAR Collaboration, Nucl. Phys. A 757, 102-183 (2005), nucl-ex/0501009; J. Adams et al, the STAR Collaboration, nucl-ex/0606014.
- [48] J. Adams et al, the STAR Collaboration, nucl-ex/0601042.
- [49] J. Adams et al, the STAR Collaboration, Phys. Rev. C 71, 064902 (2005), nucl-ex/0412019.
- [50] J. Adams et al, the STAR Collaboration, Phys. Lett. B 612, 181 (2005), nucl-ex/0406003.
- [51] S. S. Adler et al, the PHENIX Collaboration, Phys. Rev. C 72, 014903 (2005), nucl-ex/0410012.
- [52] J. Adams et al, the STAR Collaboration, Phys. Rev. Lett. 97, 132301 (2006), nucl-ex/0604019; S. Salur, Ph.D. thesis, Yale University, 2006.
- [53] R. Witt (for the STAR Collaboration), proceedings of the 19th International Conference on Ultra-Relativistic Nucleus-Nucleus Collisions (QM 2006), nucl-ex/0701063.
- [54] S.-L. Blyth (for the STAR Collaboration), nucl-ex/0608019.
- [55] S. Salur (for the STAR Collaboration), 22nd Winter Workshop on Nuclear Dynamics Talk Proceedings, nucl-ex/0606006.
- [56] J. Harris, Overview of First Results from Star, (for STAR Collaboration), Quark Matter 2002.
- [57] C. Adler et al, the STAR Collaboration, Phys. Rev. Lett. 89, 092301 (2002).
- [58] K. Adcox et al, the PHENIX Collaboration, Phys. Rev. Lett. 89, 092302 (2002).
- [59] M. Blicher et al, Phys. Rev. Lett. 88, 202501 (2002).
- [60] J. Zimanyi et al, Talk given at 30th International Symposium on Multiparticle Dynamics (ISM D 2000), Tihany, Lake Balaton, Hungary, 9-15 Oct 2000, hep-ph/0103156.
- [61] S. S. Adler et al, the PHENIX Collaboration, Phys. Rev. Lett. 91, 182301 (2003), nucl-ex/0305013; J. Adams et al, the STAR Collaboration, Phys. Rev. Lett. 95, 122301 (2005), nucl-ex/0504022.
- [62] J. H. Chen et al, Phys. Rev. C 74, 064902 (2006), nucl-th/0504055.
- [63] M. I. Pavkovic, Phys. Rev. D 13, 2128-2138 (1976).
- [64] B. Q. Ma, I. Schmidt and J. J. Yang, Phys. Lett. B 477, 107-113 (2000), hep-ph/9906424.
- [65] G. Penner and U. Mosel, Phys. Rev. C 66, 055211 (2002), nucl-th/0207066.
- [66] S. L. Zhu, W. Y. P. Hwang and Y. B. Dai, Phys. Rev. C 59, 442-450 (1999), nucl-th/9809033.
- [67] W. Rarita and J. Schwinger, Phys. Rev. 60, 61-61 (1941).
- [68] V. Shklyar, G. Penner and U. Mosel, hep-ph/0301152.